Improved microwave dielectric properties of $MgAl_2O_4$ spinel ceramics through $(Li_{1/3}Ti_{2/3})^{3+}$ doping

Xiao Li(李潇)[1], Xizhi Yang(杨习志)[1], Yuanming Lai(赖元明)[1,†], Qin Zhang(张芹)[2], Baoyang Li(李宝阳)[1], Cong Qi(戚聪)[1], Jun Yin(殷俊)[1], Fanshuo Wang(王凡硕)[1], Chongsheng Wu(巫崇胜)[1], and Hua Su(苏桦)[2]

[1] *School of Mechanical and Electrical Engineering, Chengdu University of Technology, Chengdu* 610059, *China*

[2] *State Key Laboratory of Electronic Thin Films and Integrated Devices, University of Electronic Science and Technology of China, Chengdu* 610054, *China*

(Received 2 June 2022; revised manuscript received 12 July 2022; accepted manuscript online 18 July 2022)

A series of nominal compositions $MgAl_{2-x}(Li_{1/3}Ti_{2/3})_xO_4$ ($x = 0$, 0.04, 0.08, 0.12, 0.16, and 0.20) ceramics were successfully prepared via the conventional solid-state reaction route. The phase compositions, microstructures, and microwave dielectric properties were investigated. The results of x-ray diffraction (XRD) and scanning electron microscopy (SEM) showed that a single phase of $MgAl_{2-x}(Li_{1/3}Ti_{2/3})_xO_4$ ceramics with a spinel structure was obtained at $x \leq 0.12$, whereas the second phase of $MgTi_2O_5$ appeared when $x > 0.12$. The cell parameters were obtained by XRD refinement. As the x values increased, the unit cell volume kept expanding. This phenomenon could be attributed to the partial substitution of $(Li_{1/3}Ti_{2/3})^{3+}$ for Al^{3+}. Results showed that $(Li_{1/3}Ti_{2/3})^{3+}$ doping into $MgAl_2O_4$ spinel ceramics effectively reduced the sintering temperature and improved the quality factor (Q_f) values. Good microwave dielectric properties were achieved for a sample at $x = 0.20$ sintering at 1500 °C in air for 4 h: dielectric constant $\varepsilon_r = 8.78$, temperature coefficient of resonant frequency $\tau_f = -85$ ppm/°C, and $Q_f = 62300$ GHz. The Q_f value of the $x = 0.20$ sample was about 2 times higher than that of pure $MgAl_2O_4$ ceramics (31600 GHz). Thus, $MgAl_{2-x}(Li_{1/3}Ti_{2/3})_xO_4$ ceramics with excellent microwave dielectric properties can be applied to 5G communications.

Keywords: microwave dielectric ceramics, $MgAl_2O_4$ ceramic co-substitution, $MgTi_2O_5$, solid solubility limit

PACS: 77.22.–d, 77.84.–s **DOI:** 10.1088/1674-1056/ac81a8

1. Introduction

With the rapid development of fifth-generation (5G) communication, the low signal delay and dielectric loss of electronic devices are receiving attention. As one of the core materials for these electronic devices, microwave dielectric ceramics have been wildly applied in antennas, filters, oscillators, etc.[1–3] Therefore, in order to obtain better performance for electronic devices, high-performance microwave dielectric ceramics are urgently required. Excellent microwave dielectric ceramics include a low dielectric constant ($\varepsilon_r \leq 10$), a high quality factor (Q_f), and a near-zero temperature coefficient of resonant frequency (τ_f).[4–7] The low ε_r value has the capability to reduce the signal propagation delay time effectively.[8] High Q_f values play an important role in enhancing frequency selective characteristics and suppressing signal attenuation.[9] Moreover, in order to maintain stability at a wide range of temperatures, the materials are required to have a near-zero τ_f value.[10]

$MgAl_2O_4$, a cubic spinel-type ceramics with a classic spinel structure (AB_2O_4 type), has an Fd-3m (227) space group, where Mg^{2+} and Al^{3+} ions occupy both tetrahedral and octahedral positions. They have received much attention in the field of microwave ceramics due to their low ε_r and high Q_f values. The microwave dielectric properties of $MgAl_2O_4$ were obtained with $\varepsilon_r = 8.75$, $Q_f = 68900$ GHz, and $\tau_f = -75$ ppm/°C.[11] However, the high sintering temperature (∼ 1600 °C) limits their further application in 5G communications.[12] In recent years, trivalent cations substitution of the Al-site has been focused on for spinel-type $MgAl_2O_4$. Ga^{3+} is an ideal substitute for Al^{3+} because it has similar properties to Al^{3+} in $MgAl_2O_4$ ceramics. However, it is not suitable for practical applications due to its high cost.[13] In addition, the co-substitution system with the general formula of $(M_{0.5}Ti_{0.5})^{3+}$ (M = Mg, Zn) also effectively improves the microwave dielectric properties and the sintering temperature in $MgAl_2O_4$ ceramics. $MgAl_{2-x}(Mg_{0.5}Ti_{0.5})_xO_4$ ceramics show remarkable microwave dielectric properties at 1425 °C ($\varepsilon_r = 9.1$, $Q_f = 98000$ GHz, $\tau_f = -61.36$ ppm/°C).[12] The Q_f value of $MgAl_2O_4$ and spinel-type $ZnAl_2O_4$ ceramics has been significantly improved via $(Zn_{0.5}Ti_{0.5})^{3+}$ co-substitution.[5,14,15] Furthermore, the sintering temperature of $ZnAl_2O_4$ ceramics can be reduced (below ∼ 150 °C).[5] Li^+ (0.760 Å) and Zn^{2+} (0.740 Å) have an approximately equal ionic radius and volatile properties.[16] Thus, it is expected that microwave dielectric and sintering properties are enhanced by $(Li_{1/3}Ti_{2/3})^{3+}$ co-substitution for Al^{3+} in $MgAl_2O_4$ ceramics. In this work, the influences of $(Li_{1/3}Ti_{2/3})^{3+}$ on sintering behavior, phase compositions, microstructures, and microwave dielectric properties were investigated in $MgAl_2O_4$ ceramics.

†Corresponding author. E-mail: laiyuanming19@cdut.edu.cn

© 2023 Chinese Physical Society and IOP Publishing Ltd

2. Experimental procedure

The $MgAl_{2-x}(Li_{1/3}Ti_{2/3})_xO_4$ ($x = 0$, 0.04, 0.08, 0.12, 0.16, and 0.20) ceramics were synthesized via the conventional solid-state reaction method. Firstly, MgO (99%), Al_2O_3 (99%), Li_2CO_3 (99%), and TiO_2 (99%) powders were weighted based on the calculated ratios. The weighted powders were ball-milled with zirconia balls in deionized water for 4 h. The mixed slurry was dried at 100 °C and then calcined at 1450 °C for 4 h in air. The obtained sample powders were ball-milled and dried again. Then, the calcined powders were mixed with a polyvinyl alcohol (PVA, 10 wt%) solution, and pressed into a cylinder with a diameter of 12 mm and a thickness of 6 mm under a pressure of 20 MPa. Finally, the pills were sintered in the temperature range of 1450 °C–1550 °C for 4 h. For the comparison of experimental results, pure $MgAl_2O_4$ ($x = 0$) was sintered at 1500 °C for 4 h as a control group.

Phase compositions of the ceramics were identified by Cu K_α radiation at room temperature using powder x-ray diffraction (XRD, Miniflex 600, Rigaku, Japan) in the range of 2θ from 10° to 120° with a step of 0.02°. The microstructure was obtained via XRD data refinement using the FullProf program.[17] The grain size and morphology of thermal etched samples (150 °C below that of the sintering temperature) were observed by scanning electron microscopy (SEM, JSM-6490; JEOL, Japan) at an accelerating voltage of 20 kV. The compositions of different grains were analyzed by energy dispersive spectroscopy (EDS). The relative density ($\rho_{relative}$) was used to evaluate the densification of the ceramics system, which can be calculated by using the following formula:[12,18]

$$\rho_{relative} = \frac{\rho_{bulk}}{\rho_{theo}}, \tag{1}$$

where the bulk density (ρ_{bulk}) was calculated by the Archimedes principle, and the theoretical density (ρ_{theo}) was determined via the following equation:[12,18,19]

$$\rho_{theo1,2} = \frac{A \times Z}{V \times N}, \tag{2}$$

$$\rho_{theo} = (\omega_1 + \omega_2)\left(\frac{\omega_1}{\rho_{theo1}} + \frac{\omega_2}{\rho_{theo2}}\right)^{-1}, \tag{3}$$

where V, N, A, and Z are the volume of the unit cell, Avogadro number, atomic weight, and the number of atoms in the unit cell, respectively. ω_1, ω_2, ρ_{theo1}, and ρ_{theo2} represent the weight fraction and theoretical density of each phase. The ε_r, Q_f, and τ_f values were evaluated by Hakki–Coleman dielectric resonant method. The τ_f value of each sample was calculated using the following equation:[19]

$$\tau_f = \frac{f(T_1) - f(T_2)}{(T_1 - T_2) \times f(T_2)} \times 10^6, \tag{4}$$

where $f(T_1)$ and $f(T_2)$ represent the resonant frequency at 85 °C and 25 °C, respectively.

3. Results and discussion

3.1. Phase composition and microstructure

Figure 1 shows XRD patterns of $MgAl_{2-x}(Li_{1/3}Ti_{2/3})_xO_4$ ($x = 0$, 0.04, 0.08, 0.12, 0.16, and 0.20) ceramics sintered at 1500 °C for 4 h. As shown in Fig. 1(a), the peaks of the $MgAl_{2-x}(Li_{1/3}Ti_{2/3})_xO_4$ ($x \leq 0.12$) ceramics corresponded to a single phase with spinel structure, which indicates that the $(Li_{1/3}Ti_{2/3})^{3+}$ successfully enters the inner lattice of the $MgAl_2O_4$ (PDF #75-1799) crystal. The peaks at 26° and 32° can be observed as the second phase ($MgTi_2O_5$ (PDF #76-2373)) for $x > 0.12$. The $MgTi_2O_5$ content exhibits a positive correlation with the x value. This result suggests that the solid solubility limit of $(Li_{1/3}Ti_{2/3})^{3+}$ in the $MgAl_{2-x}(Li_{1/3}Ti_{2/3})_xO_4$ ceramic was approximately at $x = 0.12$. Moreover, the diffraction peak of (311) shifts to lower angles with the increase of x value in Fig. 1(b), which indicates that expansion of the lattice has occurred.

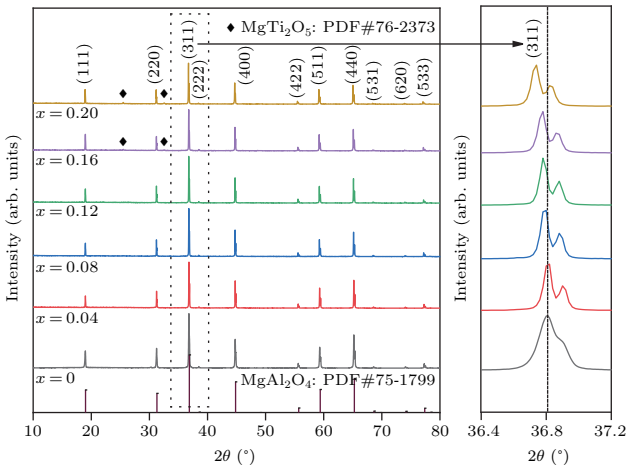


Fig. 1. XRD patterns of the $MgAl_{2-x}(Li_{1/3}Ti_{2/3})_xO_4$ ceramics sintered at 1500 °C.

To further investigate the crystal structure of $MgAl_{2-x}(Li_{1/3}Ti_{2/3})_xO_4$ ceramics, the XRD data were refined using the FullProf program. The refined patterns for $x = 0.04$ and $x = 0.20$ samples are shown in Fig. 2 (other refined XRD patterns are exhibited in the supplementary material as Fig. S1) and the Rietveld refinement results are listed in Table 1. All fitted curves agree well with the experimental data, and the positions of the Bragg reflections are consistent with the indexed peaks.

Table 1. The crystal structure parameters and density of $MgAl_{2-x}(Li_{1/3}Ti_{2/3})_xO_4$ ceramics sintered at 1500 °C.

Parameter	$x = 0$	$x = 0.04$	$x = 0.08$	$x = 0.12$	$x = 0.16$	$x = 0.20$
$a = b = c$ (Å)	8.085	8.090	8.094	8.096	8.100	8.104
$\alpha = \beta = \gamma$ (°)	90	90	90	90	90	90
V (Å^3)	528.524	529.392	530.345	530.727	531.529	532.304
ρ_{bulk} (g/cm^3)	3.379	3.404	3.449	3.458	3.441	3.424
ρ_{theo} (g/cm^3)	3.576	3.578	3.580	3.584	3.586	3.589
$\rho_{relative}$ (%)	94.5	95.2	96.4	96.5	96.0	95.5

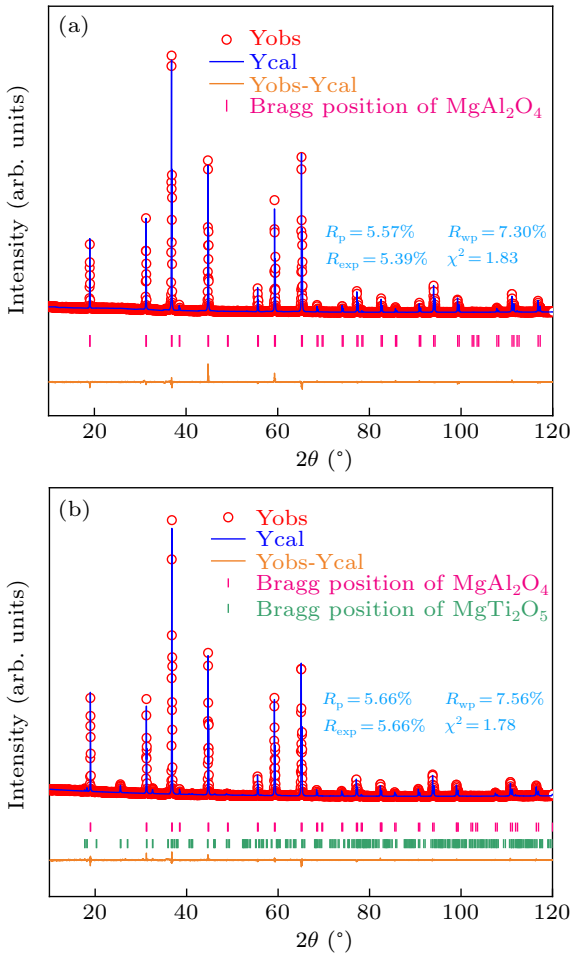


Fig. 2. Rietveld refinement of XRD patterns for $MgAl_{2-x}(Li_{1/3}Ti_{2/3})_xO_4$ ceramics sintered at 1500 °C: (a) $x = 0.04$ and (b) $x = 0.20$.

As shown in Table 1, the lattice parameters of the $MgAl_2O_4$ crystal gradually increased from 8.085 Å to 8.104 Å. The maximum cell volume value is 532.304 Å^3, which is obtained at $x = 0.20$ for the sintering temperature of 1500 °C. To further explore the changes in microstructure, the schematic diagram of ions substitution is depicted in Fig. 3. When $x \leq 0.12$, to satisfy the charge conservation, the Al^{3+} ions are partial substituted by $(Li_{1/3}Ti_{2/3})^{3+}$ ions. The equivalent ionic radius for $(Li_{1/3}Ti_{2/3})^{3+}$ can be calculated by using the following formula:[20]

$$R_{av} = \frac{1}{3}R(Li^+) + \frac{2}{3}R(Ti^{4+}) = 0.657\ \text{Å}, \tag{5}$$

where the radii of Li^+ and Ti^{4+} are 0.760 Å and 0.605 Å, respectively. The explanation for the rise in the lattice parameters is that the ionic radius of $(Li_{1/3}Ti_{2/3})^{3+}$ (0.657 Å) is larger than that of Al^{3+} (0.535 Å). When $x > 0.12$, Ti^{4+} reaches the solid solution limit in $MgAl_{2-x}(Li_{1/3}Ti_{2/3})_xO_4$ ceramics. The excess Ti^{4+} with Mg^{2+} and O^{2-} form the second phase ($MgTi_2O_5$). At this time, Li^+ enters the spinel lattice to undergo ionic substitution, which can also cause lattice expansion. In addition, the presence of Li^+ on both tetrahedral and octahedral sites, as well as an increase of the amount of Al^{3+} on the tetrahedral sites, occurs with the increase of the amount of Li.[16] Therefore, with the addition of $(Li_{1/3}Ti_{2/3})^{3+}$, it leads to an increase in the unit cell volume in the $MgAl_{2-x}(Li_{1/3}Ti_{2/3})_xO_4$ ceramics. This corresponds to the lower angle shift of the diffraction peak in the XRD pattern in Fig. 1.

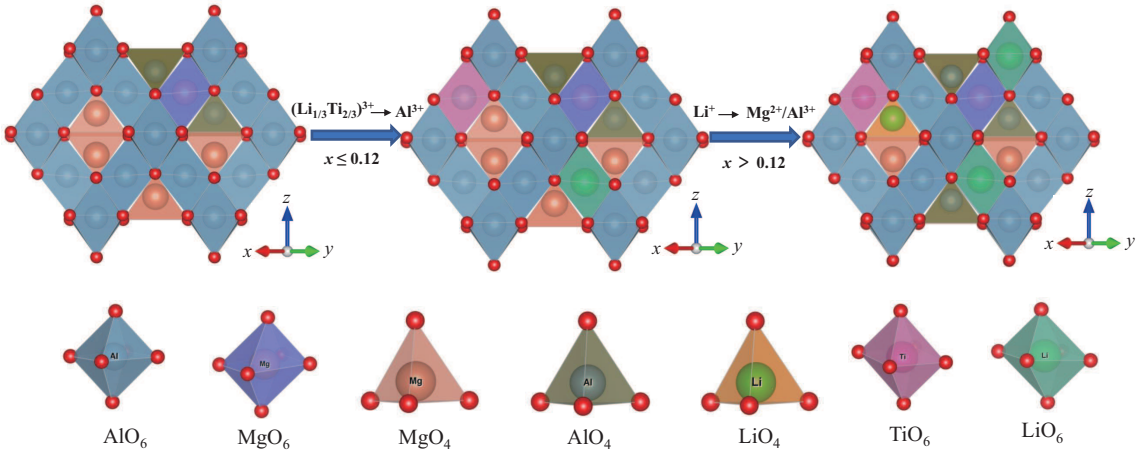


Fig. 3. The schematic crystal structure diagram for $MgAl_2O_4$ and $MgAl_{2-x}(Li_{1/3}Ti_{2/3})_xO_4$.

The SEM images of the thermal-etched surfaces for $MgAl_{2-x}(Li_{1/3}Ti_{2/3})_xO_4$ ceramics are displayed in Fig. 4. The microstructure of the samples sintered at 1500 °C is well crystallized with different compositions (Figs. 4(a)–4(d)), which is consistent with the relative density in Table 1. It is clearly seen that the rod-like structures with an average length of about 15 μm appear in the SEM image when $x = 0.20$. In addition, when x is constant, the size of the rod-like structures increase with the increase of the sintering temperature (Figs. 4(d)–4(f)). To determine the composition of the rod-like structures, two positions were selected for EDS analysis in Fig. 5(a). The corresponding results are presented in Figs. 5(b) and 5(c). Area 1 in Fig. 5(b) is proven to be the $MgAl_{2-x}(Li_{1/3}Ti_{2/3})_xO_4$ solid solutions as the ratio of Mg:Al is about 1:2. Moreover, a small amount of Ti^{4+} element could also be detected (Li cannot be detected by EDS), indicating a solid solution is formed in this

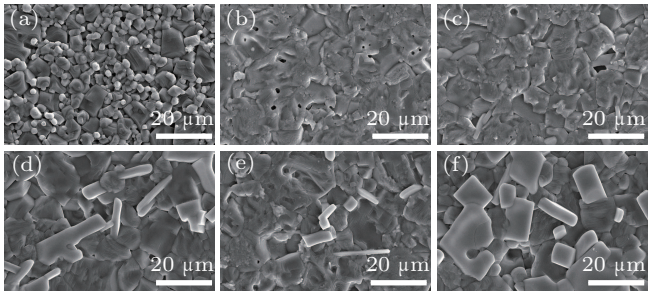


Fig. 4. SEM images of $MgAl_{2-x}(Li_{1/3}Ti_{2/3})_xO_4$ ceramics: (a) $x = 0$ sintered at 1500 °C; (b) $x = 0.04$ sintered at 1500 °C; (c) $x = 0.12$ sintered at 1500 °C; (d) $x = 0.20$ sintered at 1500 °C; (e) $x = 0.20$ sintered at 1450 °C and (f) $x = 0.20$ sintered at 1550 °C.

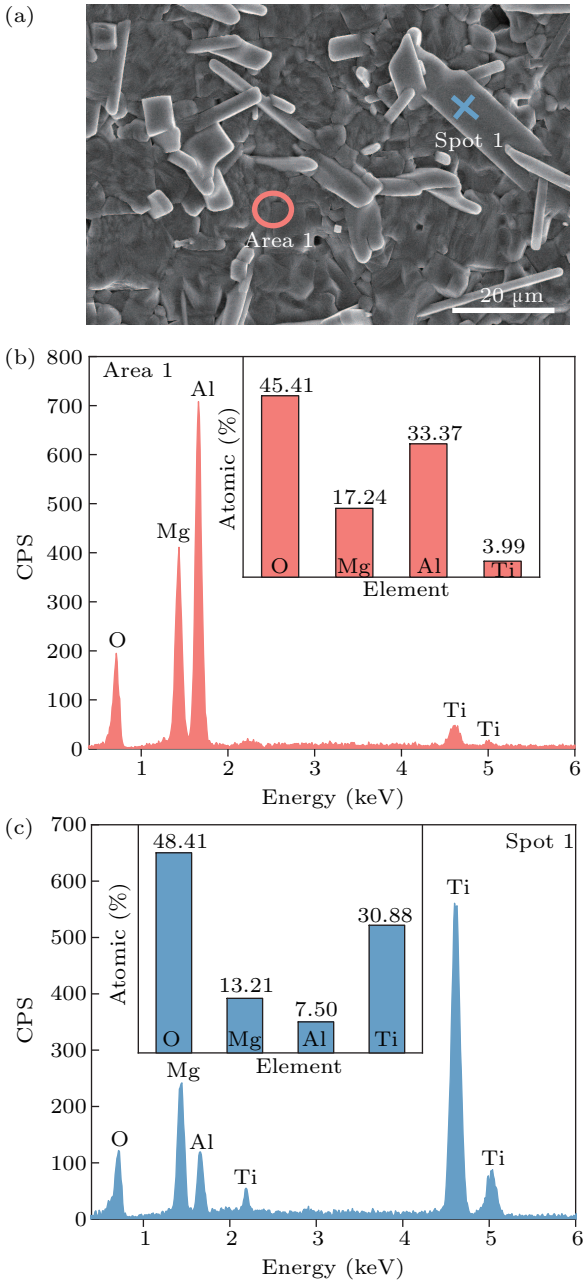


Fig. 5. (a) EDS patterns of samples at $x = 0.20$ sintered at 1500 °C; (b) EDS result analysis at area 1; (c) EDS result analysis at spot 1.

area. The rod-like structures contain a large amount of Ti element and the Mg:Ti ratio of spot 1 in Fig. 5(c) is about 1:2. Combined with XRD, SEM and EDS analysis, the rod-like structures are considered to be the second phase of $MgTi_2O_5$ and they increase with the content of $(Li_{1/3}Ti_{2/3})^{3+}$. In addition, the outward volatile diffusion of Li^+ forms a surface region with enhanced diffusion along the grain boundaries because of the volatilization of Li^+ at high temperatures, which promotes grain growth and is one of the reasons for the size gradual increase in the rod-like structures.[16,21,22]

3.2. Microwave dielectric properties

Figure 6(a) demonstrates the variation in the ε_r of the $MgAl_{2-x}(Li_{1/3}Ti_{2/3})_xO_4$ ceramics sintered at 1450 °C–1550 °C. With the increase of the x value, the ε_r value clearly increases. It reaches a maximum when $x = 0.20$ at the sintering temperature of 1450 °C, but it is still with a low dielectric constant (below 10). In general, ε_r values are mainly affected by relative density, ionic polarizability and the second phase.[23,24] For $x \leq 0.12$ samples, the ε_r values revealed the same trend as the relative density shown in Fig. 6(b). This implies that the variation of ε_r values was dominated by relative density. When $x > 0.12$, the $MgTi_2O_5$ contents increase with the increase of the x value. This is because the $MgTi_2O_5$ phase has a larger ε_r value (~ 17.4) than that of $MgAl_2O_4$ (~ 7.9).[25,26] At this point, the second phase is the crucial factor that affects ε_r values.

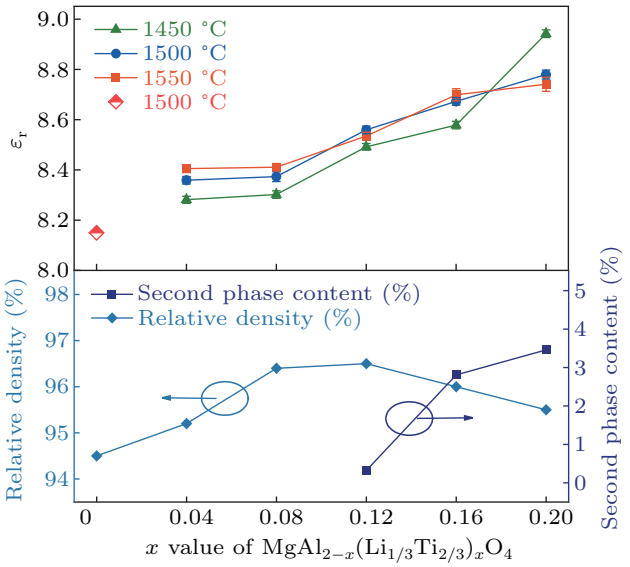


Fig. 6. The ε_r values, relative density and the second phase content: (a) ε_r values of $MgAl_{2-x}(Li_{1/3}Ti_{2/3})_xO_4$ ceramics sintered at different temperatures; (b) relative density and the second phase content of $MgAl_{2-x}(Li_{1/3}Ti_{2/3})_xO_4$ ceramics sintered at 1500 °C.

The Q_f value of the $MgAl_{2-x}(Li_{1/3}Ti_{2/3})_xO_4$ ceramics increases from 31600 GHz ($x = 0$) to 62300 GHz ($x = 0.20$) sintered at 1500 °C, as shown in Fig. 7(a). The effect of $(Li_{1/3}Ti_{2/3})^{3+}$ co-substitution on the Q_f value of $MgAl_2O_4$ can be discussed in two aspects: extrinsic factors and intrinsic factors. The primary intrinsic factors are lattice vibration

and bond characteristics, whereas the extrinsic factors generally include the densification and second phase.[27–29] To evaluate the bond characteristics of $MgAl_{2-x}(Li_{1/3}Ti_{2/3})_xO_4$ samples, the relationship between the bond strength (s) and the covalency (f_c) between cations and oxygen ions can be used to calculate the covalency of the Al-site bond in octahedral sites, which can be calculated using the following rule formula:[29–33]

$$s = \left(\frac{R_{avg}}{R}\right)^{-N}, \tag{6}$$

$$f_c = as^M, \tag{7}$$

$$\text{the degree of covalency}\ (\%) = \frac{f_c}{s} \times 100, \tag{8}$$

where R_{avg} is the average bond length between the cation and oxygen ion. R and N are empirical constants that depend on the cation site. Moreover, a and M are empirical constants that depend on the number of electrons. The relationship between the covalency of the cation-oxygen bonds and the Q_f value is displayed in Fig. 7(b), and they show the same variation trend. It can be concluded that the covalency of the Al-site bond in octahedral sites is an extremely critical factor affecting the Q_f value.

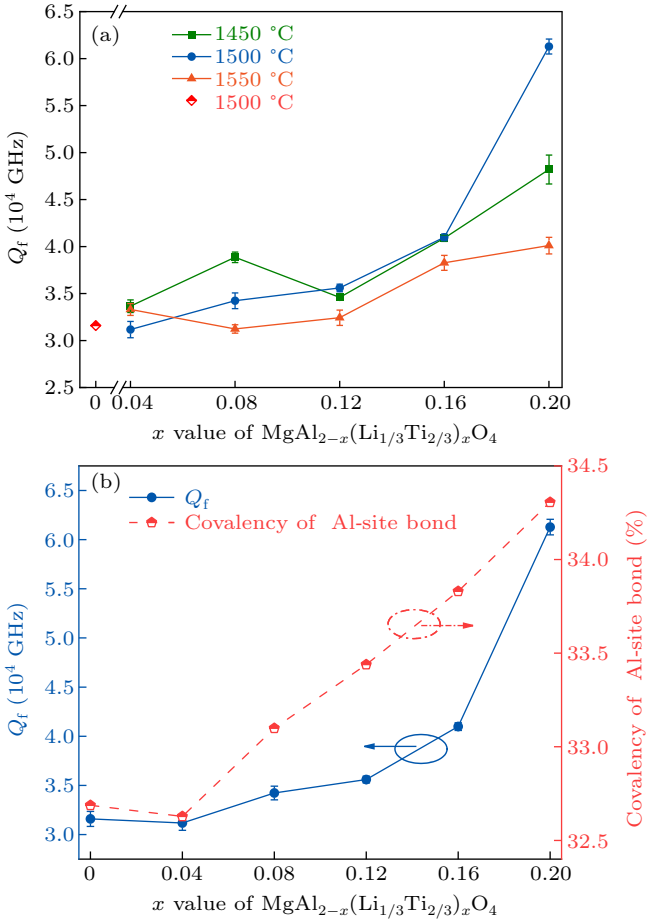


Fig. 7. Q_f values and covalency: (a) Q_f values of $MgAl_{2-x}(Li_{1/3}Ti_{2/3})_xO_4$ ceramics sintered at different temperatures; (b) Q_f values and the covalency of the Al-site bond in octahedral sites of $MgAl_{2-x}(Li_{1/3}Ti_{2/3})_xO_4$ ceramics sintered at 1500 °C.

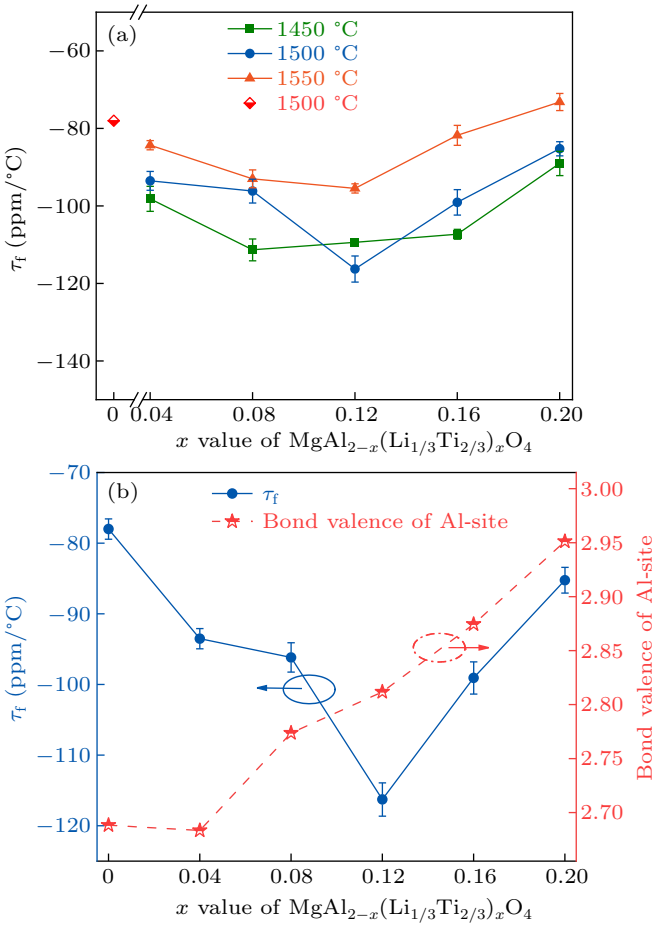


Fig. 8. τ_f values and bond valence: (a) τ_f values of $MgAl_{2-x}(Li_{1/3}Ti_{2/3})_xO_4$ ceramics sintered at different temperatures; (b) τ_f value and the bond valence of the Al-site in octahedral positions of $MgAl_{2-x}(Li_{1/3}Ti_{2/3})_xO_4$ ceramics sintered at 1500 °C.

Figure 8(a) illustrates τ_f values of $MgAl_{2-x}(Li_{1/3}Ti_{2/3})_xO_4$ ceramics sintered at 1450 °C–1550 °C. With the increase of x values, the τ_f value decreases from −78 ppm/°C to −116 ppm/°C as the x value gradually increases from 0 to 0.12, and then increases to −85 ppm/°C. Generally, the τ_f values are closely related to the bond valence and the second phase. The bond valences are calculated as follows:[34–36]

$$V_i = \sum_j v_{ij}, \tag{9}$$

$$v_{ij} = \exp\left(\frac{R_{ij} - d_{ij}}{b}\right), \tag{10}$$

where R_{ij} is the bond valence parameter, d_{ij} is the length of a bond between atoms i and j, and b is a universal constant (0.37 Å).[37] Figure 8(b) demonstrates the relationship between the bond valence of the Al-site in octahedral positions and τ_f values of the sample at 1500 °C. The τ_f values decrease first and then increase with the increase of x values. As the bond valence of the Al-site increases, the bond strength increases. Therefore, the growth of the Al-site bond valence is beneficial to the stability of the structure.[38] This is reflected in the reduction of the τ_f values. The expected opposite trend between τ_f values and the bond valences of the

Al-site is presented for samples at $x \leq 0.12$, which indicates that the τ_f values of the $MgAl_{2-x}(Li_{1/3}Ti_{2/3})_xO_4$ ceramics are mainly influenced by the bond valence. However, the τ_f values shift towards a positive correlation with the bond valences when $x > 0.12$. At this time, the second phase is the main reason for the increase of τ_f values because the τ_f value of $MgTi_2O_5$ (~ -66 ppm/°C) is larger than that of $MgAl_2O_4$ (~ -78 ppm/°C).[39]

4. Conclusion

In this study, $MgAl_{2-x}(Li_{1/3}Ti_{2/3})_xO_4$ ($x = 0$, 0.04, 0.08, 0.12, 0.16, and 0.20) ceramics have been successfully obtained by the solid-state method at 1450 °C–1550 °C. The XRD patterns indicated that a single phase with a classic spinel structure (Fd-3m) formed when $x \leq 0.12$. However, the second phase was observed when $x > 0.12$. The second phase was confirmed as $MgTi_2O_5$ and the $(Li_{1/3}Ti_{2/3})^{3+}$ was successfully inserted into the $MgAl_2O_4$ lattice by XRD refinement and EDS results. In addition, SEM showed that the $(Li_{1/3}Ti_{2/3})^{3+}$ and sintering temperature can promote $MgTi_2O_5$ grain growth. The ε_r values increased with the increase of $(Li_{1/3}Ti_{2/3})^{3+}$ content, which were mainly affected by the relative density and the second phase, but the ε_r remained below 10. The Q_f values were dominated by the average covalency of the Al-site bond in octahedral positions. Moreover, the bond valences of the Al-site and the second phase were found to be the primary factors influencing the τ_f values. Finally, the good microwave dielectric properties were achieved for samples at $x = 0.20$, sintered at 1500 °C ($\varepsilon_r = 8.78$, $Q_f = 62300$ GHz and $\tau_f = -85$ ppm/°C). The sintering temperature of the sample decreased by about 100 °C. Therefore, $MgAl_{2-x}(Li_{1/3}Ti_{2/3})_xO_4$ ceramics with good microwave dielectric properties now show great potential for applications in 5G communications.

Acknowledgment

Project supported by the Chengdu University of Technology (Grant No. KYQD2019_07728).

References

[1] Chen Y, Xue S, Luo Q, Su H, Chen Q, Huang Z, Xu L, Cao W and Huang Z 2017 *Chin. Phys. B* **26** 047701
[2] Liu Y H, Peng H Y, Yao X G, Mao M M, Song K X and Lin H X 2022 *J. Adv. Dielectr.* **12** 2250004
[3] Li Y, Xu B, Xia S and Shi P 2020 *J. Adv. Dielectr.* **10** 2050027
[4] Lai Y M, Zeng Y M, Han J, Liang X F, Zhong X L, Liu M Z, Duo B and Su H 2020 *J. Eur. Ceram. Soc.* **41** 2602
[5] Lan X K, Li J, Zou Z Y, Xie M Q, Fan G F, Lu W Z and Lei W 2019 *J. Am. Ceram. Soc.* **102** 5952
[6] Synkiewicz M B, Szwagierczak D, Kulawik J, Pałka N and Bajurko P R 2020 *J. Eur. Ceram. Soc.* **40** 362
[7] Li Y X, Fu R, Gao M Y, Chen M S, Peng R and Lu Y C 2021 *J. Electron. Mater.* **50** 3372
[8] Liu B, Sha K, Zhou M F, Song K X, Huang Y H and Hu C C 2021 *J. Eur. Ceram. Soc.* **41** 5170
[9] Lai Y M, Su H, Wang G, Tang X L, Huang X, Liang X F, Zhang H W, Li Y X, Huang K and Wang X R 2019 *J. Am. Ceram. Soc.* **102** 1893
[10] Du K, Song X Q, Zou Z Y, Fan J, Lu W Z and Lei W 2020 *Mater. Res. Bull.* **129** 110887
[11] Surendran K P, Bijumon P V, Mohanan P and Sebastian M T 2005 *Appl. Phys. A* **81** 823
[12] Qin T Y, Zhong C W, Qin Y, Tang B and Zhang S R 2020 *Ceram. Int.* **46** 19046
[13] Kan A, Okazaki H, Takahashi S and Ogawa H 2018 *Jpn. J. Appl. Phys.* **57** 11UE03-1
[14] Yang F, Lai Y M, Zeng Y M, Zhang Q, Han J, Zhong X L and Su H 2021 *Ceram. Int.* **47** 22522
[15] Surendran K P, Santha N, Mohanan P and Sebastian M T 2004 *Eur. Phys. J. B* **41** 301
[16] Blaakmeer E S, Rosciano F and van Eck E R H 2015 *J. Phys. Chem. C.* **119** 7565
[17] Juan R C 1993 *Phys. B* **192** 55
[18] Burhan U, Lei W, Yao Y F, Wang X C, Wang X H, Rehman M and Lu W Z 2018 *J. Alloys Compd.* **763** 990
[19] Jing X L, Tang X L, Tang W H, Jing Y L, Li Y X and Su H 2019 *Appl. Phys. A* **125** 415
[20] Otto H H 2015 *World J. Condens. Matter Phys.* **05** 160
[21] Qin T Y, Zhong C W, Shang Y, Cao L, Wang M X, Tang B and Zhang S R 2021 *J. Alloys Compd.* **886** 161278
[22] Reimanisa I E and Kleebeb H J 2007 *Int. J. Mater. Res.* **98** 1273
[23] Kim E S, Chun B S and Yoon K H 2003 *Mater. Sci. Eng. B-Adv.* **99** 93
[24] Ramarao S D and Murthy V R K 2013 *Scr. Mater.* **69** 274
[25] Zhou H F, Huang J, Tan X H, Wang K G, Sun W D and Ruan H 2017 *J. Mater. Sci.: Mater. Electron.* **28** 17009
[26] Shin H, Shin H K, Jung H S, Cho S Y and Hong K S 2005 *Mater. Res. Bull.* **40** 2021
[27] Kim E S, Chun B S, Freer R and Cernik R J 2010 *J. Eur. Ceram. Soc.* **30** 1731
[28] Kiran S R, Sreenivasulu G, Murthy V R K, Subramanian V and Murty B S 2012 *J. Am. Ceram. Soc.* **95** 1973
[29] Jo H J and Kim E S 2016 *J. Eur. Ceram. Soc.* **36** 1399
[30] Brown B I D and Shannon R D 1973 *Acta Crystallogr. Sect. A: Cryst. Phys. Diffr. Theor. Gen. Crystallogr.* **29** 266
[31] Takahashi S, Kan A and Ogawa H 2017 *J. Eur. Ceram. Soc.* **37** 1001
[32] Kan A, Ogawa H and Ohsato H 2007 *Jpn. J. Appl. Phys.* **46** 7108
[33] BROWN B I D and Wu K K 1976 *Acta Crystallogr. Sect. B: Struct. Crystallogr. Cryst. Chem.* **32** 1957
[34] Li J, Fang L, Luo H, Tang Y and Li C C 2016 *J. Eur. Ceram. Soc.* **36** 2143
[35] Brown B I D and Altermatt D 1985 *Acta Crystallogr. Sect. B: Struct. Sci.* **41** 244
[36] Chen M D, Zhou Z H and Hu S Z 2002 *Chin. Sci. Bull.* **47** 978
[37] Brese N E and O'Keeffe M 1991 *Acta Crystallogr. Sect. B: Struct. Sci. Cryst. Eng. Mater.* **47** 192
[38] Song X Q, Du K, Li J, Lan X K, Lu W Z, Wang X H and Lei W 2019 *Ceram. Int.* **45** 279
[39] Liou Y C and Yang S L 2007 *Mater. Sci. Eng. B* **142** 116